

# Orbital disorder and ordering in NaTiSi<sub>2</sub>O<sub>6</sub>: <sup>29</sup>Si and <sup>23</sup>Na NMR study

Ivo Heinmaa<sup>1,\*</sup>, Riho Rästa,<sup>1</sup> Harlyn J. Silverstein<sup>2</sup>, Christopher R. Wiebe<sup>2,3</sup> and Raivo Stern<sup>1,†</sup>

<sup>1</sup>Department of Chemical Physics, National Institute of Chemical Physics and Biophysics, Akadeemia tee 23, 12618 Tallinn, Estonia

<sup>2</sup>Department of Chemistry, University of Manitoba, Winnipeg, Manitoba, R3T 2N2, Canada

<sup>3</sup>Department of Chemistry, University of Winnipeg, Winnipeg, Manitoba, R3B 2E9 Canada



(Received 11 May 2022; revised 10 July 2022; accepted 15 July 2022; published 29 August 2022)

NaTiSi<sub>2</sub>O<sub>6</sub> is an exemplary compound, showing an orbital assisted spin-Peierls phase transition at  $T_c = 210$  K. We present the results of <sup>29</sup>Si and <sup>23</sup>Na nuclear magnetic resonance (NMR) measurements of NaTiSi<sub>2</sub>O<sub>6</sub>. The use of magic angle spinning (MAS) techniques unambiguously shows that only one dynamically averaged silicon site can be seen at  $T > T_c$ . At cooling, the <sup>29</sup>Si MAS NMR spectrum shows interesting changes. Immediately below  $T_c$ , the spectrum gets very broad. Cooling further, it shows two broad lines of unequal intensities which become narrower as the temperature decreases. Below 70 K, two narrow lines have chemical shifts that are typical for diamagnetic silicates. The hyperfine couplings for the two sites are  $^{29}\text{H}_{\text{hf}} = 7.4 \text{ kOe}/\mu_B$  and  $4.9 \text{ kOe}/\mu_B$ . In the paramagnetic state at high temperature, the spin-lattice relaxation of <sup>29</sup>Si was found to be weakly temperature dependent. Below  $T_c$  the Arrhenius-type temperature dependence of the relaxation rate indicates an energy gap  $\Delta/k_B = 1000(50)$  K. In the temperature region from 120 to 300 K, the relaxation rate was strongly frequency dependent. At room temperature, we found a power law dependence  $T_1^{-1} \propto \omega_L^{-0.65(5)}$ . For  $70 \text{ K} < T < 120 \text{ K}$ , the relaxation appeared to be nonexponential, which we assigned to a relaxation due to fixed paramagnetic centers. Simulation of the magnetization recovery curve showed activation type temperature dependence of the concentration of these centers. The NMR spectrum of <sup>23</sup>Na shows the line with typical shape for the central transition of a quadrupolar nucleus. A small frequency shift of <sup>23</sup>Na resonance corresponds to a very small hyperfine coupling  $^{23}\text{H}_{\text{hf}} = 0.32 \text{ kOe}/\mu_B$ . In addition, at  $T > T_c$  the <sup>23</sup>Na spectrum shows another Lorentzian shaped resonance which we attribute to the Na sites where the quadrupolar coupling is partly averaged by ionic motion.

DOI: [10.1103/PhysRevB.106.075429](https://doi.org/10.1103/PhysRevB.106.075429)

## I. INTRODUCTION

NaTiSi<sub>2</sub>O<sub>6</sub> (NTSO) is a Mott insulator with a clinopyroxene structure [1,2] made by zigzag chains of edge sharing TiO<sub>6</sub> octahedra. The chains are separated by SiO<sub>4</sub> tetrahedra (Fig. 1). The discovery of the phase transition at  $T_c = 210$  K [1], where the high-temperature paramagnetic spin system transforms gradually into a diamagnetic state, attracted great interest [1–11]. For a modest spin-spin exchange coupling constant,  $J/k_B = 300$  K [1],  $T_c$  in NTSO is very high compared to spin-Peierls transitions in other Ti<sup>3+</sup> spin chain compounds such as TiPO<sub>4</sub> with strong intrachain coupling  $J/k_B = 965$  K, but much lower spin-Peierls transition  $T_{\text{SP}} = 111$  K [12]. The powder x-ray diffraction (XRD) data [1,2] showed that the magnetic phase transition in NTSO is accompanied by a structural phase transition, where the high-temperature phase with equal Ti-Ti distances transforms into the low-temperature phase with alternating short and long Ti-Ti distances. Similar phase transition at even higher temperature  $T_c = 230$  K has been detected in isostructural pyroxene compound LiTiSi<sub>2</sub>O<sub>6</sub> [1].

The zigzag configuration of the octahedra in the NTSO chain (Fig. 1) puts clear constraints to the coupling between  $3d^1$  electrons of Ti<sup>3+</sup> ions. A single electron of the Ti<sup>3+</sup> shell in the crystal field of a distorted octahedron can occupy three possible  $t_{2g}$  orbitals:  $d_{xy}$ ,  $d_{xz}$ , and  $d_{yz}$ . It was considered that at high temperature,  $T > T_c$ , due to the equal Ti-Ti distances, the lowest two energy levels are degenerate while the latter orbital at a bit higher energy is almost unoccupied. At low temperature, the two lowest energy levels become unequal, leading the system into a dimerized and diamagnetic ground state with a singlet-triplet gap  $\Delta = 53$  meV (615 K) [3].

In an early description of a one-dimensional (1D) zigzag chain, Hikihara and Motome [5] pointed out two most probable configurations of Ti<sup>3+</sup> spin- and orbital-ordering patterns: (i) the nearest neighbors have spin-ferro and orbital-antiferro configuration and (ii) the neighbors have spin-antiferro (spin-dimer) and orbital-ferro configuration. The first case favors the Hund's rule coupling and is consistent with equal Ti-Ti distances in the chain, whereas the second case favors the superexchange interaction, spin-singlet state of the dimers and alternating Ti-Ti distances. Originally, the authors proposed [5] that at  $T_c$  the orbital order changes from the pattern (i) to the pattern (ii).

*Ab initio* calculations of NTSO [10,11,13,14] showed that below  $T_c$  the spin-dimer coupling is favored, whereas at high temperature they proposed that the  $d$  electron of Ti occupies

\*ivo.heinmaa@kbfi.ee

†raivo.stern@kbfi.ee

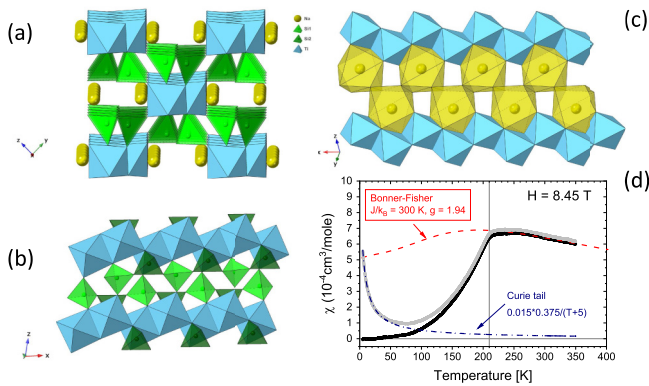


FIG. 1. Crystal structure of  $\text{NaTiSi}_2\text{O}_6$  at 100 K [(a)–(c)] [2]. Edge shared  $\text{TiO}_6$  octahedra (blue) form zigzag chains which are separated by  $\text{SiO}_4$  tetrahedra (light green and dark green), Na ions are forming two rows between zigzag chains. Unlike the high-temperature structure, which has a single silicon ion in its unit cell, the low-temperature structure has two different silicon ions. In panel (b), the dimer  $d_{xz}$  orbitals lie in  $xz$  plane, the drawing plane. The two oxygens of Si1 tetrahedra (light green) are connected to the two neighboring Si2 tetrahedra (dark green), and the other two oxygens are connected to three  $\text{Ti}^{3+}$  ions of two dimers. The Si2 tetrahedra have two nearest neighbor Si1 tetrahedra and three nearest  $\text{Ti}^{3+}$  ions, but the  $d_{xz}$  orbital of the third  $\text{Ti}^{3+}$  is orthogonal to the oxygen of Si2 tetrahedron, and most probably does not contribute to the spin density at Si2.  $\text{Na}^+$  ions are surrounded by eight nearest oxygen ions as shown in panel (c), four of which are connected to three nearest  $\text{TiO}_6$  octahedra, four have connection to the neighboring  $\text{NaO}_8$  polyhedra. The magnetic susceptibility curve of NTSO is given in panel (d). The raw data are the dark gray curve, the blue dash-dotted line is the curve corresponding to the Curie tail ascribed to  $\approx 1.5\%$  localized impurities. The black line corresponds to the susceptibility after subtracting the Curie tail. The red dashed line corresponds to the susceptibility of homogeneous Heisenberg antiferromagnetic chain [16] for exchange interaction between the neighbors,  $J/k_B = 300$  K, known as the Bonner-Fisher curve [17].

more or less equally all three  $t_{2g}$  states. Recent DFT calculations showed [8] that involvement of the third  $t_{2g}$  orbital and oxygen-atom-mediated electron hopping comparable to the direct hopping integral between neighboring Ti atoms results in much stronger quantum fluctuations. The authors calculated the energy levels and hopping integrals for several orbital configurations of zigzag chain and found similar results: At low-temperature structure the AF spin configuration is stable by about 20 meV whereas for high-temperature structure the AF and FM configurations are almost degenerate.

Using their heat conductivity measurements, Rivas-Murias *et al.* [7] reported an interesting finding—in the wide temperature region 150–300 K, the heat conductivity shows glass-like behavior. The behavior was attributed to the rapid orbital fluctuations above  $T_c$  in an orbital-liquid state.

Recently, the local structure of NTSO was studied by x-ray and neutron diffraction using atomic pair distribution function (PDF) method [15]. The PDF method allows detecting of local interatomic distances without the need to have long-range order and has been used to detect local dimers in many similar dimerized compounds [9]. Koch *et al.* [15] established two different Ti-Ti distances above  $T_c$  similar to the case at low

$T$  and concluded that on warming above  $T_c$  the dimers evolve into a short-range orbital degeneracy lifted (ODL) state persisting up to temperature at least 490 K. The proposed ODL state involves local segments (domains) of  $xy$  dimers and  $zx$  dimers separated by domain walls consisting of  $\text{Ti}^{3+}$  ions with antiferro-orbital couplings of occupied  $yz$  orbitals or ions of occupied mixed orbitals  $zx-xy$ .

Nuclear magnetic resonance techniques are known to provide valuable information about the local order and local dynamics of spins. In this paper, we explore NTSO using the  $^{29}\text{Si}$  and  $^{23}\text{Na}$  nuclear magnetic resonance (NMR).

## II. EXPERIMENTAL

A polycrystalline sample of  $\text{NaTiSi}_2\text{O}_6$  was prepared by a solid-state reaction as described in Ref. [3]. The MAS NMR measurements were carried out on a Bruker AVANCE-II-360 spectrometer at 8.45 T external magnetic field (resonance frequency 71.44 MHz for  $^{29}\text{Si}$  and 95.119 MHz for  $^{23}\text{Na}$ ) using a home-built cryoMAS probe for  $15 \times 1.8$  mm  $\text{Si}_3\text{N}_4$  rotors [19,20]. The spectra were recorded with  $\pi/2 - \tau - \pi - \tau - \text{echo}$  pulse sequence where the delay  $\tau$  was set to one rotor period. In the whole temperature region, the sample spinning frequency was adjusted to 30 kHz. The temperature of the fast-rotating sample was measured with a temperature sensor (LakeShore Cernox) at spinner assembly and corrected using an earlier calibration of the temperature dependence of  $^{207}\text{Pb}$  chemical shift for  $\text{Pb}(\text{NO}_3)_2$ . The frequency shifts for  $^{29}\text{Si}$  and  $^{23}\text{Na}$  are given respective to tetramethylsilane (TMS) and NaCl resonances, respectively. We used the line-shape analysis provided by the Bruker TopSpin program. The spin-lattice relaxation  $T_1$  was found to be almost equal in rotating sample and static sample. Therefore,  $T_1$  has been measured on static sample with saturation-recovery pulse sequence. The magnetic susceptibility was measured with physical property measurement system (PPMS) (Quantum Design) vibrating sample magnetometer (VSM) at 8.45 T, the same field strength as NMR spectra were recorded. Additional  $T_1$  measurements were performed in Bruker magnets of 4.7 and 11.7 T as well as at various fields of the PPMS.

## III. RESULTS

### A. $^{29}\text{Si}$ MAS NMR spectra

Temperature dependence of the  $^{29}\text{Si}$  MAS NMR spectrum is given in Fig. 2. At  $T = 320$  K, the spectrum shows a single Lorentzian line at 707 ppm with a width (FWHM) of 57 ppm. With decreasing temperature, the isotropic Knight shift follows the temperature dependence of the magnetic susceptibility. At the phase transition, the resonance line broadens abruptly. In a spectrum recorded at 188 K, another line (line B) at smaller Knight shift is clearly seen. At lower temperatures, the spectrum shifts to the diamagnetic direction, the lines become narrower, the intensity of the line B increases and that of the line A decreases. At temperature 57 K, the spectrum shows two narrow lines at  $-100$  and  $-117$  ppm (typical range of silicon chemical shifts of silicates [21]) with the widths of 8.3 and 7.5 ppm, respectively. Following the study of the  $^{29}\text{Si}$  chemical shifts in titanosilicates [22], one

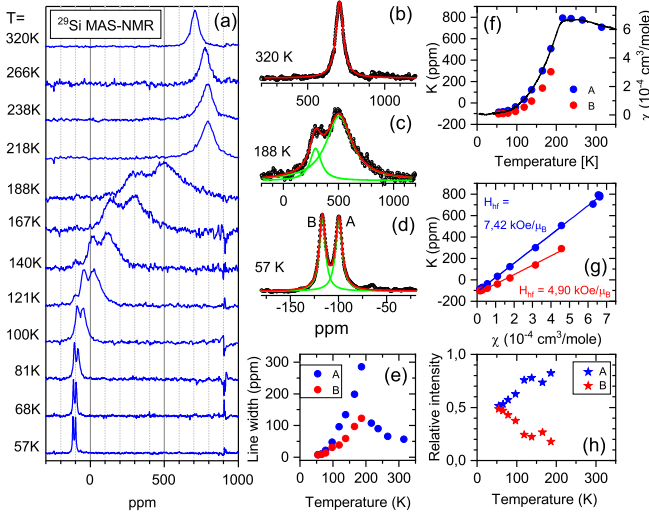


FIG. 2. (a) The temperature dependence of the  $^{29}\text{Si}$  MAS NMR spectrum of  $\text{NaTiSi}_2\text{O}_6$ . (b) The spectrum at 320 K can be well fitted by a single Lorentzian line. (c) Below the phase transition, the spectrum consists of two broad Lorentzian lines with unequal intensities. (d) At low temperature, the spectrum contains two narrow Lorentzian lines, denoted by A and B, of equal intensities and widths; the temperature dependence of the lines width and relative intensities are given in panels (e) and (h). (f) The Knight shift of both lines is proportional to the magnetic susceptibility. (g) For the lines A and B, two different hyperfine couplings are obtained from the Clogston-Jaccarino plot [18].

should expect that the silicon with effectively two nearest neighbor  $\text{Ti}^{3+}$  ions can be assigned to the line at  $-117$  ppm, and the line at  $-110$  ppm belongs to silicon with effectively three nearest  $\text{Ti}^{3+}$  neighbors. The Knight shift of both lines follows linearly the magnetic susceptibility curve:

$$K(T) = K_0 + \frac{H_{\text{hf}}}{N_A \mu_B} \chi. \quad (1)$$

Here,  $K_0$  is the temperature-independent shift, the chemical shift, and  $H_{\text{hf}}$  is the hyperfine coupling constant. From a Clogston-Jaccarino plot [18] [Fig. 2(g)],  $K$  vs  $\chi$ , we determined the hyperfine couplings  $^{29}\text{H}_{\text{hf}} = 7.42$  and  $4.90$  kOe/ $\mu_B$  for A and B resonances, respectively.

### B. $^{29}\text{Si}$ spin-lattice relaxation

$^{29}\text{Si}$  spin-lattice relaxation  $T_1$  was measured using static sample and saturation-recovery pulse sequence. At temperatures above the phase transition,  $T > 210$  K, the magnetization recovery was single exponential. Due to inhomogeneous broadening at temperatures below the phase transition, the magnetization recovery at different positions of the broad line showed different  $T_1$  values. The data in Fig. 3 are measured at the maximum and show almost single exponential magnetization recovery. The temperature dependence of the relaxation rate is given in the main panel of Fig. 3. The relaxation rate at  $T > 210$  K is only weakly dependent on temperature as expected for ordinary paramagnetic compounds. According to Moriya [23], the relaxation in paramagnetic state at high

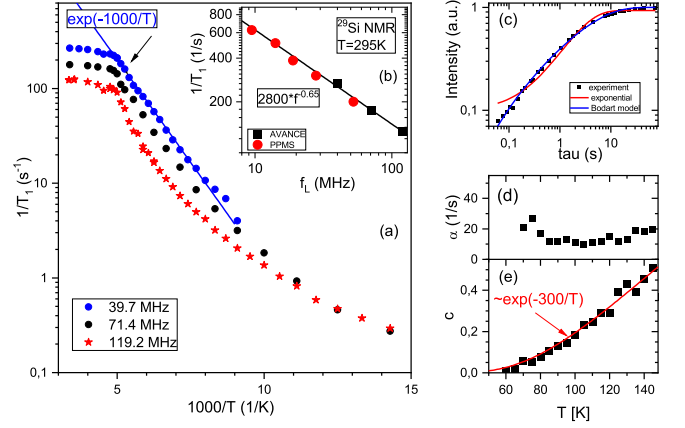


FIG. 3. Temperature dependence of the  $^{29}\text{Si}$  spin-lattice relaxation rate as measured from the recovery of the intensity at maximum of the line (a). The inset (b) shows the frequency (field) dependence of the relaxation rate at  $T = 295$  K. Here, the data at high frequencies (black squares) are measured on AVANCE spectrometers at fixed field, and the low-frequency data are measured in the adjustable magnetic fields of PPMS. In panel (c), we show typical nonexponential recovery of the  $^{29}\text{Si}$  magnetization at temperatures below 120 K, where the red line shows exponential recovery, and the blue line corresponds to the magnetization recovery due to paramagnetic centers in the model by Bodart *et al.* [24] (Eq. (3); see text). Panel (d) shows the temperature dependence of amplitude  $\alpha$  from the fit to the nonexponential recovery, and the panel (e) shows the temperature dependence of the concentration  $c$  from the same fit (see text). The red line in panel (e) corresponds to the fit to the temperature dependence of the concentration of paramagnetic centres.

temperature can be given as

$$\frac{1}{T_1} = \frac{2\gamma_N^2 \sqrt{2\pi} I(I+1)}{3\omega_E z'} H_{\text{hf}}^2, \quad (2)$$

where  $\gamma_N$  is the nuclear gyromagnetic ratio,  $I$  is the nuclear spin,  $H_{\text{hf}}$  is the total hyperfine coupling as in Eq. (1),  $z' = 3$  is the number of the nearest paramagnetic neighbors next to the nucleus, the Heisenberg exchange frequency is given as  $\omega_E = (|J|k_B/\hbar)\sqrt{2zS(S+1)}/3$  (in units of  $\text{rad s}^{-1}$ ), where  $z = 2$  (in present case) is the number of nearest neighbor  $\text{Ti}^{3+}$  ions,  $S = 1/2$  is the electronic spin, and  $J$  is the magnitude of the exchange interaction (in Kelvin). Taking the hyperfine coupling  $H_{\text{hf}} = 7.42$  kOe/ $\mu_B$  from Clogston-Jaccarino plot [Fig. 2(g)] and  $J/k_B = 300$  K, we obtain the high temperature relaxation rate  $T_1^{-1} = 102$   $\text{s}^{-1}$ , which is a right order of magnitude as seen in Fig. 3. An interesting finding of a strong dependence of the relaxation rate on the  $^{29}\text{Si}$  Larmor frequency  $f_L$  (e.g., applied magnetic field) as  $T_1^{-1} \propto f_L^{-2/3}$  [see Fig. 3(b)] will be discussed below.

Below the phase transition, the relaxation rate decreases quickly, with activation-type decay  $T_1^{-1} \propto \exp(-1000/T)$ . The activation-type decay of the relaxation rate has been recorded in several spin-Peierls compounds [25–27] and is caused by the opening of an energy gap in the spectrum of magnetic fluctuations. For the fully dimerized spin  $1/2$  Heisenberg AF chain the singlet-triplet gap value  $\Delta = J/k_B$  is expected. Here we attribute the fast relaxation decay to the fast activation type decay of the magnetic hyperfine shift  $K(T)$

as  $T_1^{-1} \propto K(T)^2$ . This will give us  $K(T) \propto \exp(-500/T)$  and, according to Eq. (1), we have  $\chi(T) \propto \exp(-500/T)$ . From this we get an estimate of the excitation gap as  $\Delta = 500$  K and intradimer exchange energy as  $J/k_B = 500$  K.

In the temperature range  $70 < T < 140$  K, the nuclear magnetization recovery becomes nonexponential with typical  $\propto t^{1/2}$  time dependence in the beginning of the recovery. Such behavior has been assigned to the relaxation mechanism due to paramagnetic impurities [28]. The mechanism has been analyzed by two groups [24,29], who provided almost identical models for the description of the process. In this so-called Bodart model, the magnetization recovery is given by two parameters—the concentration of the relaxation centers,  $c$ , and the amplitude of the relaxation source  $\alpha$ :

$$\frac{M_0 - M_Z(t)}{M_0} = \frac{1}{1 - c} [F(c^2 \alpha t) - cF(\alpha t)], \quad (3)$$

where  $F(x) = e^{-x} - \sqrt{\pi x} \operatorname{erfc}(\sqrt{x})$ , with the complementary error function  $\operatorname{erfc}(z) = \frac{2}{\sqrt{\pi}} \int_z^\infty e^{-t^2} dt$ . It is noted that the actual meaning of the concentration  $c$  and the amplitude  $\alpha$  are related to the symmetry of the structure. In addition, the formulas are valid within a certain region of concentrations—the model does not work on high concentrations, since the relaxation centers need to be diluted, and in our case, it does not work at very low concentration, since we have  $\approx 1\%$  of paramagnetic impurities from synthesis. We assumed the description is valid in the temperature region, where the parameter  $\alpha$  is reasonably constant. Using this formalism, we obtained the parameters  $\alpha$  and  $c$  from the fit to the nonexponential magnetization recovery curves in the temperature region from 60 to 140 K. Typical nonexponential magnetization recovery curve is given in Fig. 3(c). One can see that the model given by Eq. (3) perfectly describes experimental curve. The temperature dependence of the parameter  $c$  (proportional to the concentration of paramagnetic centers in the lattice) and the parameter  $\alpha$  are given in Figs. 3(e) and 3(d), respectively. Figure 3(e) shows that in noted temperature region the concentration of the paramagnetic centers decreases by more than an order of magnitude, while the parameter  $\alpha$  is almost constant in the region between 60 to 140 K. Thus, we consider this temperature region valid for the measurements of the concentration of fixed paramagnetic centers. The temperature curve of the concentration is given in Fig. 3(e). It is well reproduced by the activation law  $c \propto \exp(-E_a/T)$ , with  $E_a/k_B = 300$  K. Surprisingly, the activation energy for excitation of the centers is almost two times lower than 600 K, which is needed for creation of broken singlets [3]. Therefore, we believe the paramagnetic centers we see in the relaxation originate from orbital disorder in the structure such as domain walls between the ordered sequences in the zigzag chain, between *zigzag* and *zagzig* orders, as proposed in Feiguin *et al.* [8] and Koch *et al.* [15]. The situation resembles the well-known case of domain walls in the Su-Schiffer-Heeger model of polyacetylene [31]. We carried out similar measurements of the concentration of paramagnetic centers in three different magnetic fields: 14.1, 8.5, and 4.7 T magnetic fields [Fig. 3(a)]. In all three measurements, the activation energy was essentially the same,  $E_a/k_B = 300 \pm 20$  K.

### C. $^{23}\text{Na}$ MAS NMR

$^{23}\text{Na}$  is a quadrupolar nucleus with a spin  $I = \frac{3}{2}$  and with an electric quadrupolar moment  $Q$ . The term in the nuclear Hamiltonian corresponding to the quadrupolar interaction is usually given [32,33] as

$$\mathcal{H}_Q = \frac{eQV_{zz}}{4I(2I-1)} \left[ 3I_z^2 - I(I+1) + \frac{\eta}{2}(I_+^2 + I_-^2) \right], \quad (4)$$

where the spin operators have their usual notations,  $V_{\alpha\alpha}$  ( $\alpha = x, y, z$ ) denote the principal components of the electric field gradient (EFG) tensor  $\mathbf{V}$ , with the convention  $|V_{xx}| \leq |V_{yy}| \leq |V_{zz}|$ , and  $eQ$  is the nuclear quadrupolar moment. The asymmetry parameter  $\eta$  is defined as  $\eta = (V_{xx} - V_{yy})/V_{zz}$ .

The NMR spectrum of a quadrupolar nucleus gives unique information about the local charge distribution outside the ion. In an external magnetic field, the nuclear Hamiltonian for a nucleus with a spin  $\frac{3}{2}$  has  $2I + 1 = 4$  eigenstates (noted as  $m = -\frac{3}{2}, -\frac{1}{2}, +\frac{1}{2}, +\frac{3}{2}$ ) and three allowed transitions [ $m \leftrightarrow (m \pm 1)$ ] between the states. The energy levels of the eigenstates depend on the quadrupolar interaction, which is characterized by the quadrupolar coupling constant  $C_q = (e^2qQ)h$  ( $eq = V_{zz}$ ), and the asymmetry parameter  $\eta$ . In the case of cubic symmetry of local charges, the EFG is zero, the energy levels of the nuclear Hamiltonian are equidistant, the energy of all transitions equals to the Zeeman energy (including chemical shift, dipolar shift etc), and the NMR spectrum consists of a single line at the Larmor frequency like in the case of a  $I = \frac{1}{2}$  nucleus. In case the local charge distribution is not cubic, the NMR spectrum of a spin  $I = \frac{3}{2}$  nucleus shows three lines corresponding to the transitions called satellite transitions ( $m = \pm\frac{3}{2} \leftrightarrow \pm\frac{1}{2}$ ) and central transition ( $m = -\frac{1}{2} \leftrightarrow +\frac{1}{2}$ ). The position of the central transition line occurs around the Larmor frequency, and those of the satellite transitions lines about  $\pm C_q$  away from the Larmor frequency, depending on the orientation of the external magnetic field in the frame of the quadrupolar coupling tensor. Although the line of the central transition occurs close to the Larmor frequency, it is shifted by the quadrupolar interaction in second order. Therefore, in powder samples, it shows a peculiar double horn shape. In the MAS NMR experiment, this line is substantially narrowed, but the peculiar line shape is still characterizing the quadrupolar couplings. The analysis of that shape allows determination of the quadrupolar coupling parameters.

In the structure of NTSO, there is one sodium ion in a unit cell, which has eight oxygen nearest neighbors [Fig. 1(c)]. Since the local symmetry is not cubic, the EFG at  $^{23}\text{Na}$  nuclei is finite, and the NMR spectrum is influenced by the quadrupolar interaction as described above. As it turns out, the resonance lines of satellite transitions in powder sample are too broad ( $C_q \approx 3.1$  MHz) to be observed in MAS NMR experiment, but the central transition can be easily measured. Simulation of the line shape gives the values of the Knight shift, the quadrupolar coupling constant, and the asymmetry of the EFG tensor. The temperature dependence of the Knight shift and the quadrupolar coupling parameters are given in Figs. 4(e) and 4(f). At high temperature, we detected another, featureless resonance line with considerable relative intensity

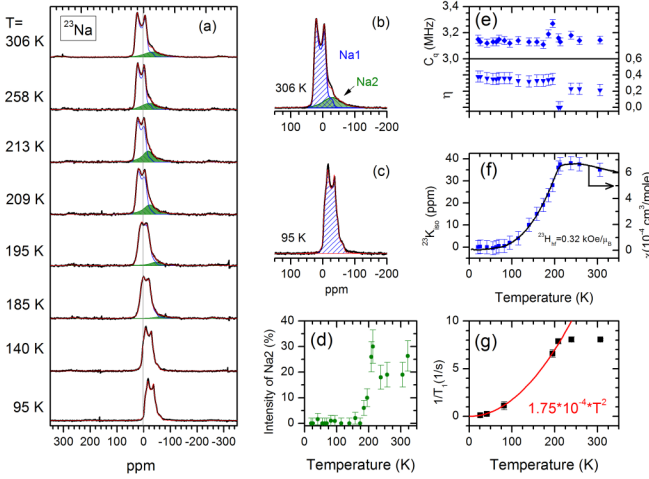


FIG. 4. Temperature dependence of the  $^{23}\text{Na}$  MAS NMR spectrum of NTSO: (a) the black line is the recorded spectrum; the red line corresponds to the fitting. The detailed view of the spectrum at 306 K (b) shows two resonances corresponding to Na sites denoted as Na1 (blue stripes) and Na2 (green); the line corresponding to Na1 sites has typical double horn shape of central transition of quadrupolar nucleus in a powder sample, whereas the resonance corresponding to the sites Na2 has featureless Gaussian-Lorentzian shape. Below the phase transition, the spectrum shows only one Na1 line (c). Temperature dependence of relative intensity of the Na2 resonance is shown in panel (d). Panel (e) shows temperature dependences of the quadrupolar coupling constant,  $C_q$ , and the asymmetry parameter,  $\eta$ , as fitting parameters to the Na1 line shape. Panel (f) shows that temperature dependence of the isotropic value of magnetic shift  $^{23}K_{\text{iso}}$  (blue squares) scales perfectly with the temperature dependence of the magnetic susceptibility  $\chi$  (full line). The hyperfine coupling  $^{23}H_{hf} = 0.32 \text{ kOe}/\mu_B$  was obtained from  $^{23}K_{\text{iso}}$  vs  $\chi$  plot. Temperature dependence of sodium spin lattice relaxation rate  $1/T_1$  is given in panel (g).

of  $\approx 25\%$  [Fig. 4(b)]. This line we assigned to a sodium ion where the quadrupolar coupling is partially averaged due to fluctuation of the EFG. Below  $T_c$ , this line disappears [Figs. 4(c) and 4(d)]. Almost temperature-independent quadrupolar coupling constant is in accord with very weak temperature dependence of the mean Na-O bond length, decreasing from  $d_{\text{mean}} = 2.424 \text{ \AA}$  at 300 K to  $d_{\text{mean}} = 2.416 \text{ \AA}$  [2]. The spin lattice relaxation of  $^{23}\text{Na}$  [Fig. 4(g)] shows a weak temperature dependence at  $T > T_c$  due to fluctuations of paramagnetic spins, like the relaxation of  $^{29}\text{Si}$ . At lower temperatures, the relaxation follows  $1/T_1 \propto T^2$  dependence as typical for quadrupolar nuclei relaxing due to the Raman mechanism of lattice vibrations [32].

## IV. DISCUSSION

### A. Orbital disorder below $T_c$

The single resonance line in  $^{29}\text{Si}$  MAS NMR (Fig. 2) of NTSO indicates that either (i) there is only one silicon site in the lattice or (ii) the different surroundings of silicon are averaged by fast orbital fluctuations. The case (i) is clearly in contradiction with recent observations by x-ray PDF experiments [15], which clearly established different Ti-Ti distances at temperature far above  $T_c$ . Therefore, the single resonance of

$^{29}\text{Si}$  must be a result of (ii), a motional narrowing [30]. Here we did not mention the possibility that in magnetic compounds some resonances may be invisible due to silicon sites with the large static hyperfine field or due to fast relaxation. The sites with large static hyperfine fields can be ignored because this would need some different  $\text{Ti}^{3+}$  sites in the lattice, which are not observed by x-ray [2]. In addition, magnetically different  $\text{Ti}^{3+}$  sites would show up in the  $K$  vs  $\chi$  plots, which are perfectly linear for the isotropic hyperfine shift for  $^{29}\text{Si}$ , and for  $^{23}\text{Na}$  as well. Too fast  $T_1$  or  $T_2$  relaxation could be excluded by the same reasons. Taking the full linewidth in rigid lattice as 300 ppm ( $= 21.3 \text{ kHz}$ ) equal to the value immediately below  $T_c$  [Figs. 2(b) and 2(e)], we get an estimate to the correlation time of orbital fluctuations in high-temperature structure as  $\tau_c < 10^{-4} \text{ s}^{-1}$ .

According to the temperature development of the NMR spectra, below  $T_c$  this fluctuation freezes, and the spectrum shows static disorder, a distribution of magnetic shifts in a rigid lattice. The ordering gradually develops with decreasing temperature. At around  $T \approx 130 \text{ K}$ , the two different silicon sites are well seen, and thus we can consider this temperature as the temperature where the low-temperature structure is established. At cooling further, the NMR lines become narrower as the number of paramagnetic  $\text{Ti}^{3+}$  ions decreases. Dynamic and static orbital disorder in the region of  $130 \text{ K} < T < 300 \text{ K}$  is in good agreement with glass-like behavior of heat conductivity in this temperature region [7].

The assignment of the lines A and B in the  $^{29}\text{Si}$  NMR low-temperature spectrum to the two silicon sites in the low-temperature structure of NTSO (Fig. 1) can be done as given above: The line A belongs to the site Si1, where the silicon is effectively connected to three  $\text{Ti}^{3+}$  ions; and the line B to the site Si2, connected effectively to two nearest neighbor  $\text{Ti}^{3+}$  ions. This assignment is validated by the 3:2 ratio of the hyperfine couplings:  $^{29}H_{hf}(\text{Si1}) = 7.42 \text{ kOe}/\mu_B$  vs  $^{29}H_{hf}(\text{Si2}) = 4.90 \text{ kOe}/\mu_B$ .

A question remains as to why the intensity of the B line at high temperatures is much smaller compared to the A line. One possible way to explain this is to assume occupation of the third  $d$  orbital, e.g., the  $d_{yz}$  orbital involved in the configuration of the ODL state [15].

### B. Magnetic susceptibility

In Fig. 5, we show the susceptibility curve in comparison with calculated susceptibilities. As noted above, the high-temperature susceptibility is very well described by the calculation within the Bonner-Fisher model [16,17], in good agreement with the previous measurement [1]. Here we used the coupling parameter  $J/k_B = 300 \text{ K}$  and the  $g = 1.94$ , a little lower than  $g = 2$  (typical for  $d^1$  electrons of  $\text{Ti}^{3+}$  ions in octahedral field [34]). The susceptibility for isolated dimers in Heisenberg AF chains has well-known analytical temperature curve for dimers [16]:

$$\chi(T) = \frac{N_A(\mu_B g)^2}{k_B T \left[ 3 + \exp\left(\frac{J}{k_B T}\right) \right]}, \quad (5)$$

where  $N_A$  is the Avogadro's number,  $\mu_B$  is the Bohr magneton,  $g$  is the electron  $g$  factor, and  $J$  is the intradimer exchange coupling constant. If we use the same exchange coupling

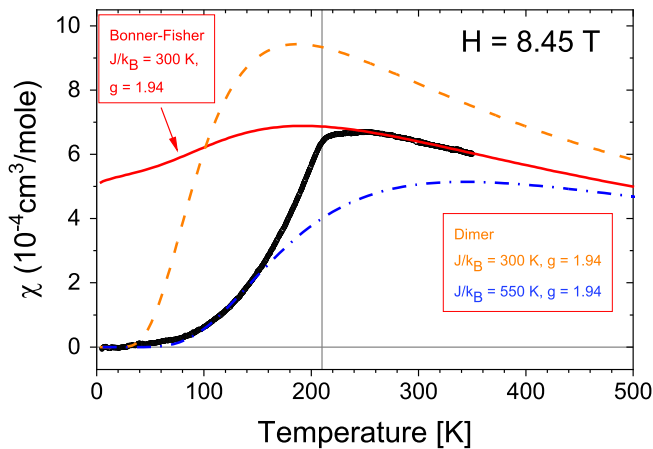


FIG. 5. Temperature dependence of the magnetic susceptibility of NTSO. The experimental curve with subtracted Curie tail (black circles) is compared to the susceptibility calculated in the Bonner-Fischer model for uniform Heisenberg antiferromagnetic chain (red line) and the susceptibility curve for isolated dimers with coupling constant  $J/k_B = 300$  K (dashed orange curve) and with  $J/k_B = 550$  K (blue dash-dotted line).

constant  $J/k_B = 300$  K in a dimer model, we reach the enhanced susceptibility as given by the dashed orange line in Fig. 5. In other words, at  $T_c$  one expects the magnetization increase. According to the NMR spectra, the low-temperature dimerized structure is set below  $T < 130$  K, where one can expect the susceptibility curve for isolated dimers being justified. Blue curve in Fig. 5 shows good fit to the experimental data using considerably higher  $J/k_B$  value of 550 K. Rather strong intradimer exchange couplings  $J/k_B$  between 396 to 626 K have been reported by first principles calculations [10,13], and are related to the short intradimer distance  $d_{T_i-T_i} = 3.08$  Å in NTSO [2], much shorter than that in dimerized  $\text{TiPO}_4$ , with  $d_{T_i-T_i} = 3.13$  Å [35], where the exchange coupling, obtained from high-temperature susceptibility curve, is even larger  $J/k_B = 965$  K [12].

### C. Spin-lattice relaxation

An interesting finding from  $^{29}\text{Si}$  spin-lattice relaxation measurements is the frequency dependence of the relaxation rate presented in Fig. 3(b) (inset). The room-temperature data show  $T_1^{-1} \propto f_L^{-0.65}$ , where  $f_L$  is the Larmor frequency. This trend was observed in the broad Larmor frequency region from 9 to 119 MHz. The temperature curves in Fig. 3(a) show that similar trend of the frequency dependence of  $T_1$  is present at temperatures down to  $\approx 130$  K. Recall that in ordinary 3D paramagnetic compounds the nuclear relaxation is independent of the Larmor frequency [23], depending only on the exchange frequency of electron spins as given above.

In 1D AF Heisenberg chains, the relaxation at low frequencies is enhanced due to 1D spin diffusion. The spin diffusion causes a low-frequency enhancement of the spectral density of spin fluctuations and is observed in the NMR relaxation as  $1/T_1 = A + B f_L^{-\frac{1}{2}}$ , where  $A$  is the relaxation due to the spin exchange as given above and  $B$  is a constant (see, e.g., Refs [36–39]). In some cases, the dependence is weaker. For example, careful muon spin relaxation  $\lambda$  measurements as a function of magnetic field  $B$  on an organic radical-ion salt with ideal  $S = 1/2$  Heisenberg AF chain showed field (frequency) dependence as  $\lambda \propto B^{-n}$  with  $n = 0.350(7)$  [40], in reasonable agreement with theory [41].

We are not aware of nuclear relaxation measurements on AF chains with orbital disorder, but it is known that any kind of disorder causes enhancement of the low-frequency spectral density as proved by proton relaxation study of spin dynamics in antiferromagnetic hetero-metallic molecular rings [42], where the authors demonstrate that in the homometallic ring  $\text{Cr}_8$ , the relaxation rate at high temperature was frequency independent, whereas in the substituted rings  $\text{Cr}_7\text{Cd}$ ,  $\text{Cr}_7\text{Ni}$  and  $\text{Cr}_7\text{Fe}$  the high-temperature relaxation became frequency dependent. It is interesting to note that “disorder” in a series of doped paratacamites (“Herbertsmithites”)  $\text{MCu}_3(\text{OH})_6\text{Cl}_2$  ( $M = \text{Zn}, \text{Mg}$ ), quantum spin liquid candidates with frustrated kagome lattice, causes frequency dependence of muon spin relaxation rate  $1/T_1 \propto \omega_L^{-0.66}$  [43,44], similar to the present case.

### V. CONCLUSION

Using  $^{29}\text{Si}$  and  $^{23}\text{Na}$  MAS NMR spectra, we have studied the orbital ordering in NTSO. Temperature dependence of the spectra shows that dynamic order at high temperature freezes at  $T_c$  into a disordered state with different local configurations of orbitals. With cooling further, the orbitals order gradually into well-defined dimers with singlet ground state. The magnetic susceptibility and spin lattice relaxation data are in accordance with relatively strong intradimer exchange coupling at low temperatures  $J/k_B = 500$  (50) K. The spin-lattice relaxation rate  $1/T_1$  was found to be strongly dependent on resonance frequency. At room temperature, we obtained  $T_1^{-1} \propto f_L^{-2/3}$  in a broad frequency region.

### ACKNOWLEDGMENTS

We would like to thank E. Joon, A. A. Tsirlin, S. V. Streltsov, and T. Giamarchi for several instructive discussions. This research was supported by the Estonian Science Council Grants No. IUT23-7 and No. PRG4, the European Regional Development Fund Grants No. TK133 and No. TK134, and the European Unions Horizon 2020 research and innovation Grant No. 871106 (ISABEL). C.R.W. and H.J.S. would like to acknowledge support through NSERC.

[1] M. Isobe, E. Ninomiya, A. N. Vasil’ev, and Y. Ueda, *J. Phys. Soc. Jpn.* **71**, 1423 (2002).

[2] G. J. Redhammer, H. Ohashi, and G. Roth, *Acta Cryst. B* **59**, 730 (2003).

- [3] H. J. Silverstein, A. E. Smith, C. Mauws, D. L. Abernathy, H. Zhou, Z. Dun, J. Van Lierop, and C. R. Wiebe, *Phys. Rev. B* **90**, 140402(R) (2014).
- [4] M. J. Konstantinović, J. van den Brink, Z. V. Popović, V. V. Moshchalkov, M. Isobe, and Y. Ueda, *Phys. Rev. B* **69**, 020409(R) (2004).
- [5] T. Hikihara and Y. Motome, *Phys. Rev. B* **70**, 214404 (2004).
- [6] P. J. Baker, S. J. Blundell, F. L. Pratt, T. Lancaster, M. L. Brooks, W. Hayes, M. Isobe, Y. Ueda, M. Hoinkis, M. Sing, M. Klemm, S. Horn, and R. Claessen, *Phys. Rev. B* **75**, 094404 (2007).
- [7] B. Rivas-Murias, H. D. Zhou, J. Rivas, and F. Rivadulla, *Phys. Rev. B* **83**, 165131 (2011).
- [8] A. E. Feiguin, A. M. Tsvelik, W.-G. Yin, and E. S. Božin, *Phys. Rev. Lett.* **123**, 237204 (2019).
- [9] E. S. Božin, W.-G. Yin, R. J. Koch, M. Abeykoon, Y. S. Hor, H. Zheng, H. C. Lei, C. Petrovic, J. F. Mitchell, and S. J. L. Billinge, *Nat. Commun.* **10**, 3638 (2019).
- [10] S. V. Streltsov and D. I. Khomskii, *Phys. Rev. B* **77**, 064405 (2008).
- [11] S. V. Streltsov and D. I. Khomskii, *Phys. Usp.* **60**, 1121 (2017).
- [12] J. M. Law, C. Hoch, R. Glaum, I. Heinmaa, R. Stern, J. Kang, C. Lee, M.-H. Whangbo, and R. K. Kremer, *Phys. Rev. B* **83**, 180414(R) (2011).
- [13] S. V. Streltsov, O. A. Popova, and D. I. Khomskii, *Phys. Rev. Lett.* **96**, 249701 (2006).
- [14] D. I. Khomskii and S. V. Streltsov, *Chem. Rev.* **121**, 2992 (2021).
- [15] R. J. Koch, R. Sinclair, M. T. McDonnell, R. Yu, M. Abeykoon, M. G. Tucker, A. M. Tsvelik, S. J. Billinge, H. D. Zhou, W.-G. Yin, and E. S. Božin, *Phys. Rev. Lett.* **126**, 186402 (2021).
- [16] D. C. Johnston, R. K. Kremer, M. Troyer, X. Wang, A. Klümper, S. L. Bud'ko, A. F. Panchula, and P. C. Canfield, *Phys. Rev. B* **61**, 9558 (2000).
- [17] J. C. Bonner and M. E. Fisher, *Phys. Rev.* **135**, A640 (1964).
- [18] J. R. Singer, *Phys. Rev.* **104**, 929 (1956); A. M. Clogston and V. Jaccarino, *ibid.* **121**, 1357 (1961).
- [19] D. Arčon, I. Heinmaa, and R. Stern, in *Modern Methods in Solid-State NMR: A Practitioner's Guide*, edited by P. Hodgkinson, New Developments in NMR Vol. 15 (Royal Society of Chemistry, Cambridge, 2018), pp. 231–261.
- [20] A. Samoson, T. Tuherm, J. Past, A. Reinhold, T. Anupöld, and I. Heinmaa, in *New Techniques in Solid-State NMR*, edited by J. Klinowski, Topics in Current Chemistry Vol. 246 (Springer, Berlin, 2005), pp. 15–31.
- [21] G. Engelhardt and D. Michel, *High Resolution Solid-State NMR of Silicates and Zeolites* (John Wiley & Sons, New York, 1987).
- [22] M. L. Balmer, B. C. Bunker, L. Q. Wang, C. H. F. Peden, and Y. Su, *J. Phys. Chem. B* **101**, 9170 (1997).
- [23] T. Moriya, *Prog. Theor. Phys.* **16**, 23 (1956); *J. Phys. Soc. Jpn.* **18**, 516 (1963).
- [24] J. R. Bodart, V. P. Bork, T. Cull, H. Ma, P. A. Fedders, D. J. Leopold, and R. E. Norberg, *Phys. Rev. B* **54**, 15291 (1996).
- [25] L. S. Smith, E. Ehrenfreund, A. J. Heeger, L. V. Interrante, J. W. Bray, H. R. Hart Jr., and I. S. Jacobs, *Solid State Commun.* **19**, 377 (1976).
- [26] M. Itoh, S. Hirashima, and K. Motoya, *Phys. Rev. B* **52**, 3410 (1995).
- [27] S. R. Saha, S. Golin, T. Imai, and F. C. Chou, *J. Phys. Chem. Solids* **68**, 2044 (2007).
- [28] G. W. Blumberg, *Phys. Rev.* **119**, 79 (1960).
- [29] A. Labouriau, Y.-W. Kim, and W. L. Earl, *Phys. Rev. B* **54**, 9952 (1996).
- [30] H. S. Gutowsky and G. E. Pake, *J. Chem. Phys.* **18**, 162 (1950).
- [31] W. P. Su, J. R. Schrieffer, and A. J. Heeger, *Phys. Rev. Lett.* **42**, 1698 (1979).
- [32] A. Abragam, *Principles of Nuclear Magnetism* (Oxford University Press, New York, 1961).
- [33] C. P. Slichter, *Principles of Magnetic Resonance* (Springer-Verlag, New York, 1992).
- [34] H. J. Gerritsen, in *Paramagnetic Resonance*, edited by W. Low (Academic Press, New York, 1963), Vol. 1, p. 3.
- [35] M. Bykov, J. Zhang, A. Schönleber, A. Wölfel, Sk. Imran Ali, S. van Smaalen, R. Glaum, H.-J. Koo, M.-H. Whangbo, P. G. Reuvekamp, J. M. Law, C. Hoch, and R. K. Kremer, *Phys. Rev. B* **88**, 184420 (2013).
- [36] F. Borsa and M. Mali, *Phys. Rev. B* **9**, 2215 (1974).
- [37] J.-P. Boucher, M. Ahmed Bakheit, M. Nechtschein, M. Villa, G. Bonera, and F. Borsa, *Phys. Rev. B* **13**, 4098 (1976).
- [38] M. Takigawa, T. Asano, Y. Ajiro, M. Mekata, and Y. J. Uemura, *Phys. Rev. Lett.* **76**, 2173 (1996).
- [39] F. Adelnia, M. Mariani, L. Ammannato, A. Caneschi, D. Rovai, R. E. P. Winpenny, G. Timco, M. Corti, A. Lascialfari, and F. Borsa, *J. Appl. Phys.* **117**, 17B308 (2015).
- [40] F. L. Pratt, S. J. Blundell, T. Lancaster, C. Baines, and S. Takagi, *Phys. Rev. Lett.* **96**, 247203 (2006).
- [41] G. Müller, *Phys. Rev. Lett.* **60**, 2785 (1988).
- [42] H. Amiri, A. Lascialfari, Y. Furukawa, F. Borsa, G. A. Timco, and R. E. P. Winpenny, *Phys. Rev. B* **82**, 144421 (2010).
- [43] J. S. Helton, K. Matan, M. P. Shores, E. A. Nytko, B. M. Bartlett, Y. Qiu, D. G. Nocera, and Y. S. Lee, *Phys. Rev. Lett.* **104**, 147201 (2010).
- [44] E. Kermarrec, P. Mendels, F. Bert, R. H. Colman, A. S. Wills, P. Strobel, P. Bonville, A. Hillier, and A. Amato, *Phys. Rev. B* **84**, 100401(R) (2011).